ACS Catalysis

Subscriber access provided by University of South Dakota

Article

Synergy between Ceria Oxygen Vacancies and Cu Nanoparticles facilitates the Catalytic Conversion of CO2 to CO under Mild Conditions

Sheng-Chiang Yang, Simon H. Pang, Taylor Sulmonetti, Wei-Nien Su, Jyh-Fu Lee, Bing-Joe Hwang, and Christopher W Jones

ACS Catal., **Just Accepted Manuscript** • DOI: 10.1021/acscatal.8b04219 • Publication Date (Web): 13 Nov 2018

Downloaded from http://pubs.acs.org on November 14, 2018

Just Accepted

"Just Accepted" manuscripts have been peer-reviewed and accepted for publication. They are posted online prior to technical editing, formatting for publication and author proofing. The American Chemical Society provides "Just Accepted" as a service to the research community to expedite the dissemination of scientific material as soon as possible after acceptance. "Just Accepted" manuscripts appear in full in PDF format accompanied by an HTML abstract. "Just Accepted" manuscripts have been fully peer reviewed, but should not be considered the official version of record. They are citable by the Digital Object Identifier (DOI®). "Just Accepted" is an optional service offered to authors. Therefore, the "Just Accepted" Web site may not include all articles that will be published in the journal. After a manuscript is technically edited and formatted, it will be removed from the "Just Accepted" Web site and published as an ASAP article. Note that technical editing may introduce minor changes to the manuscript text and/or graphics which could affect content, and all legal disclaimers and ethical guidelines that apply to the journal pertain. ACS cannot be held responsible for errors or consequences arising from the use of information contained in these "Just Accepted" manuscripts.

ACS Publications

is published by the American Chemical Society. 1155 Sixteenth Street N.W., Washington, DC 20036

Published by American Chemical Society. Copyright © American Chemical Society. However, no copyright claim is made to original U.S. Government works, or works produced by employees of any Commonwealth realm Crown government in the course of their duties.

Synergy between ceria oxygen vacancies and Cu nanoparticles facilitates the catalytic conversion of CO_2 to CO under mild conditions

Sheng-Chiang Yang,[a,b] Simon H. Pang,[a] Taylor P. Sulmonetti,[a] Wei-Nien Su,[c] Jyh-Fu Lee,[d] Bing-Joe Hwang,[b,d,*] and Christopher W. Jones[a,*]

[a] *School of Chemical & Biomolecular Engineering, Georgia Institute of Technology, 311 Ferst Drive, Atlanta, Georgia 30332, United States*

[b] *Department of Chemical Engineering, National Taiwan University of Science and Technology, 43 Keelung Rd. Sec. 4, Taipei 10617, Taiwan, R.O.C.*

[c] *Graduate Institute of Applied Science and Technology, National Taiwan University of Science and Technology, 43 Keelung Rd. Sec. 4, Taipei 10617, Taiwan, R.O.C.*

[d] *National Synchrotron Radiation Research Center, 101 Hsin-Ann Road, Hsinchu Science Park, Hsinchu 30076, Taiwan, R.O.C.*

[*]Corresponding Author: Prof. Christopher W. Jones
Tel.: +1 404 385 1683; fax: +1 404 894 2866
E-Mail: cjones@chbe.gatech.edu
Address: School of Chemical & Biomolecular Engineering, Georgia Institute of Technology, 311 Ferst Drive, Atlanta, Georgia 30332, United States

[*]Corresponding Author: Prof. Bing-Joe Hwang
Tel.: +886-2-27376624; fax: +886-2-27376644
E-Mail: bjh@mail.ntust.edu.tw
Address: Department of Chemical Engineering, National Taiwan University of Science and Technology, 43 Keelung Rd. Sec. 4, Taipei 10617, Taiwan, R.O.C.

Abstract

The performance of supported metal catalysts can depend on many factors, including metal particle size and dispersion and metal-support interactions, and differentiation of these effects is challenging due to their interwoven relationship. Copper/ceria catalysts are well known redox catalysts studied in the conversion of CO and CO_2 via oxidation and/or reduction pathways. The redox behavior of each species, Cu-CuO and CeO_x-CeO_2, are often suggested to be interlinked, allowing ceria-supported copper domains to outperform copper species on other, non-redox active supports. In this work, the catalytic activity of nano-sized Cu supported on either cerium oxide or mesoporous silica is explored using samples where the Cu weight loading, particle size and dispersion of Cu are held constant to highlight the impact of the two supports on catalytic performance without additional influencing factors. The Cu/CeO_2 catalysts are synthesized via a space-confined method to limit the growth of CeO_2 particles and to achieve a high dispersion of Cu. Through *in-situ* XRD and XAS, it is shown that the presence of Cu nanoparticles on the CeO_2 support lowers the reduction temperature of CeO_2, allowing formation of oxygen vacancies at low temperatures < 300 °C. The Cu/CeO_x catalyst demonstrates 100% CO selectivity in the low temperature (300 °C) and ambient pressure conversion of CO_2 to CO, even when approaching equilibrium conversion. Moreover, this catalyst is approximately 4 times more active than the corresponding Cu/SiO_2 catalyst with otherwise similar structural attributes. The potential reaction pathways are probed by *in-situ* FTIR and *in-situ* XAS at various temperatures, identifying Cu^+-CO species and oxygen vacancies forming under some conditions. The collected experimental evidence also suggest a reaction sequence for CO_2

hydrogenation over Cu/CeO_x catalysts, consistent with DFT reports in the literature.

Keywords: oxygen vacancies, reducible oxide support, spillover, CO_2 to CO, WGS, reverse water gas shift

1. Introduction

The increasing energy demand of modern society has significantly increased the consumption of carbon-containing fossil fuels on an unprecedented scale, which unfortunately releases a large amount of carbon dioxide into the atmosphere. CO_2 is considered as the main contributor to global warming with the concentration in air having increased to above 400 ppm.[1-2] Carbon capture and storage (CCS)[3-5] has been proposed to reduce CO_2 emissions by capturing carbon dioxide from flue gas or ambient air[6] and then injecting into the ground and storing it in different forms. Although CCS is considered technically feasible, it is not currently an adopted solution to decreasing carbon emissions due to its high cost, the risk of leakage during or after injection, as well as other factors.[7] Carbon capture and utilization (CCU)[8-10] is a parallel approach whereby the captured and separated CO_2 is used as a feedstock to produce value-added chemicals and fuels. However, conversion of CO_2 into chemicals and fuels presents challenges due to the use of expensive reductants or precious metal catalysts, low selectivity to key products, and high energy consumption due to the need for high temperature and pressure reactions.[11-12] One route to address these challenges is the reverse water-gas shift (rWGS)[13-14] reaction under mild conditions, which converts CO_2 into CO using hydrogen (ideally hydrogen generated using renewable feedstocks), at 300 °C and at ambient pressure to generate this useful chemical feedstock.

Reducible metal oxides are good candidates as catalyst supports in the rWGS reaction because their redox properties can be tuned to enhance the performance of metallic nanocatalysts.[15-17] In particular, CeO_2 can be easily thermally reduced (400-800 °C) in the presence of H_2 to create oxygen

vacancies, which have been demonstrated to assist in conversion of CO_2 to CO. However, as demonstrated by pulse injection of CO_2, once most of the Ce^{3+} is oxidized back to Ce^{4+} by CO_2 at lower temperatures, no further conversion of CO_2 to CO was observed, suggesting that the oxygen vacancies were consumed and unable to be regenerated under catalytic conditions.[18]

The catalytic performance of such materials can be further tuned by adding redox active metals such as Cu. It has been established that the ceria-supported copper nanoparticles have unique electronic and chemical properties where coupled redox character can positively impact specific applications. For preferential/oxidation of CO (CO-PR/OX),[19-22] key factors affecting the catalytic reactivity were the formation of surface oxygen vacancies, Cu^{2+}/Cu^{+} and Ce^{4+}/Ce^{3+} redox pairs, enhanced O_2 dissociation, and stabilized CO chemisorption. For the water gas shift (WGS) reaction,[23-25] similar important factors were identified, including Cu^{+}/Cu and Ce^{4+}/Ce^{3+} redox pairs, H_2O dissociation and stabilized CO chemisorption. For steam reforming (SR),[26-28] the presence of highly-dispersed Cu species, enhanced oxygen mobility, C-H bond breaking ability, and H_2O dissociation were important parameters. Finally, for methanol synthesis from CO_2,[29-32] the co-presence of Cu^{+}/Cu and Ce^{4+}/Ce^{3+} redox pairs, H_2 dissociation, stabilized CO/CO_2 chemisorption to carbonates, and the presence of C-H bond formation pathways were important factors.

By controlling the structure of the metallic domains and ceria domains, effective catalysts that operate under mild conditions, specifically low temperatures and ambient pressures, can be achieved for the above chemistries as well as related reactions. Porosoff et al.[11] discussed some state-of-the-art catalysts for the rWGS reaction under mild conditions. However, CO_2 conversions were

generally low (under 10 %) due to the stability of CO_2, with higher conversions generally requiring more harsh conditions. Previously, some of us developed an SBA-15 templating technique to prepare nanostructured Cu/CeO_2 catalysts for methanol steam reforming,[27] and further demonstrated that these materials, which contained numerous oxygen vacancies, could effectively adsorb CO_2 and convert it to CO under high temperature conditions using a pulsed titration method.[33] In this study, we have synthesized the catalyst by a similar SBA-15 templating technique and explored the use of the nanostructured Cu/CeO_2 catalysts in the rWGS reaction under atmospheric pressure and at low temperature, leveraging hydrogen spillover, the Ce^{4+}/Ce^{3+} redox pairs and CO_2 chemisorption/conversion under relatively mild conditions. The performance is compared to a traditional mesoporous silica supported copper catalyst (Cu/SBA-15)[34] with similar reduced Cu particle size.

2. Experimental Section

2.1. Catalyst Preparation

Mesoporous silica SBA-15 was synthesized in accordance with previous literature[35] except that the surfactants were removed by calcining the synthesized materials at 550 °C for 10 h. Cu/CeO_2 and CeO_2 were synthesized via a space-confined method: $Cu(NO_3)_2$ and/or $Ce(NO_3)_3$ were dissolved in 0.4 mL DI water at Cu/Ce atomic ratios of 3:7 and 0:10 and the resulting solution was placed in a vacuum oven at room temperature until a gel-like light blue salt was obtained. The salt (1 g) was mixed with 1.5 g of SBA-15 and the solid mixture was ground in a mortar and pestle. The mortar was placed

on a hot plate at 70 °C until the light blue salt dissolved into the SBA-15, and the mixture was then placed in a vacuum oven at room temperature overnight. The dried mixture was calcined in a muffle furnace by increasing the temperature from room temperature to 700 °C at a heating rate of 1 °C/min and holding for 12 h, followed by cooling to room temperature.

The silica template was removed by washing with aqueous NaOH (2 M, 75 mL) three times at 70 °C. The porous metal-oxide products were recovered by centrifugation and washed with DI water three times. The residual sodium was removed by aqueous ammonia (1 M, 50 mL), dried at 100 °C and calcined at 400 °C for 1 h. Herein, these samples are denoted as SCuCe and SCe. The copper loading in the SCuCe was quantitatively determined to be 9.0 wt% by inductively coupled plasma atomic emission spectroscopy (ICP-AES). Cu/SBA-15 was prepared by dissolving $Cu(NO_3)_2$ in a mixture of water and acetone, mixing with the as-prepared SBA-15, and holding at 60 °C for 1 h prior to heat treatment in vacuum (ca. 50 mTorr) at 350°C for 2 h with a ramp of 1 °C/min. This sample is denoted as CuSBA. The copper loading in the CuSBA was quantitatively determined to be 8.9 wt% by ICP-AES.

2.2. Catalyst Characterization

Inductively coupled plasma (ICP-AES) analysis for the quantitative determination of Cu content of these samples was conducted on a PerkinElmer OPTIMA 7300 DV.

High-resolution transmission electron microscopy (TEM) was conducted using a FEI Tecnai G2 F30 S-TWIN with a field-emission gun operating at 300 kV. The TEM was also equipped with an

X-ray energy dispersive spectrometer for elemental mapping. The specimens were prepared by dropping a methanol-catalyst dispersion on a carbon membrane-coated Ni-grid and allowing the methanol to evaporate.

Samples were characterized using X-ray powder diffraction with an in-house Philips X-pert diffractometer using Cu K radiation, or *in-situ* using synchrotron radiation at Beam Line 01C at the National Synchrotron Radiation Research Center (NSRRC), Hsinchu, Taiwan. The electron storage ring was operated at 1.5 GeV with a beam current of 100-200 mA. The XRD pattern was recorded using a wavelength of 1.5418 Å as the energy of Cu $K_{\alpha 1}$. The patterns were obtained at a scan rate of 10° min^{-1} with steps of 0.05°, from 10 to 90°. The peak positions were referenced to JCPDS cards #75-0076 (CeO_2), #85-1326 (Cu), and #80-1268 (CuO).

X-ray absorption measurements were carried out at the National Synchrotron Radiation Research Center (NSRRC), Hsinchu, Taiwan. The X-ray absorption near-edge structure (XANES) measurements at the Ce L3-edge and Cu K-edge were performed at Wiggler beamline 17C and 07A using a Lytle cell or transmission cell. A double crystal Si (111) monochromator was used with an energy resolution $\Delta E/E$ better than 2×10^{-4}. The energy resolutions were about 0.3 to 0.4 eV at Ce L3-edge (5723 eV) in the range of 5520 to 6570 eV and Cu K-edge (8979 eV) in the range of 8770 to 9840 eV. The focused beam size at the sample position was 4 mm × 2 mm. Prior to the XAS measurements, samples were fresh, reduced with 10% H_2 at 300 °C or reacted 100% CO_2 at 120 °C after H_2 reduction. The XAS data were processed and analyzed with Athena software including background removal, edge-step normalization, and Fourier transform. Artemis software was utilized

to fit the Fourier transformed EXAFS data with a model. To compensate for dampening of the EXAFS amplitude with increasing k, the normalized $\chi(E)$ was transformed from energy space to k-space. The k2-weighted $\chi(k)$ data in the k-space ranging from 3.1 to 10.1 $Å^{-1}$ for Cu K-edge, was Fourier transformed (FT) to r-space to separate the EXAFS contributions from different coordination shells. A nonlinear least squares algorithm was applied to curve fitting of EXAFS in r-space between 1.5 to 3.0 Å for Cu-Cu first shell; 0.46 to 2 Å for Cu-O first shell, depending on the bond to be fitted. The reference, copper foil was employed for the Cu-Cu bonds; Cu_2O and CuO standards were employed for Cu-O bonds. All theory models are from Feff8 file of Cu, Cu_2O and CuO.

Cu dispersion measurements by H_2/N_2O temperature programmed reduction/oxidation (TPR/O) were performed on a Micromeritics Autochem II 2920 equipped with a thermal conductivity detector (TCD). The experiment to determine total Cu content was first set with a heating rate of 7 °C min^{-1} from room temperature to 300 °C in an atmosphere comprising a 10% H_2/Ar mixture. Secondly, 10% N_2O/He was absorbed on the sample by the pulse method to achieve saturation of the surface at 50 °C. Finally, to calculate the surface area of the copper surface layer (Cu_2O), the same TPR protocol as in the first step was used. *In-situ* DRIFTS measurements were performed by using a high-temperature environmental reaction chamber supported in a Praying Mantis (Harrick) DRIFTS optical system with ZnSe windows. The spectra were collected on a Thermo Nicolet iS10 FTIR spectrometer equipped with a liquid-nitrogen-cooled MCT detector; the whole optical path was purged with CO_2- and H_2O-free nitrogen. Prior to CO_2 (1% CO_2 in He) adsorption at 35 °C, the samples were reduced by H_2 (4% H_2 in He) at 300 °C and then the backgrounds were collected to eliminate the effect of temperature for

in-situ measurements. After CO_2 adsorption (1% CO_2 in He) for 20 minutes, the experimental spectra were collected in the presence of a H_2 (4% H_2 in He) at temperatures from 35 to 300 °C. He flow was used to purge the cell between each gas change.

2.3. Catalytic Testing

The CO_2 to CO reaction via rWGS was conducted under the following conditions: a weight hourly space velocity (WHSV) of 1.12 or 4.49 h^{-1}, and a H_2/CO_2 molar ratio of 3 at 300 °C and 1 bar total pressure. The catalytic performance of the materials was tested in a fixed bed stainless steel reactor. The pelletized catalyst (58-68 μm) was placed at the center of the reactor tube between two layers of glass beads and quartz wool. All catalysts were first reduced by H_2 at 300 °C before introduction of the H_2/CO_2 mixture. The reactor effluent composition was characterized by an Agilent 7890 gas chromatograph (GC) equipped with two TCD (Molecular Sieve 5A and Hayesep column) and a flame ionization detector (PoraBond U column). The CO_2 conversion is defined as the consumed CO_2 (molar) amount divided by the input CO_2 (molar) amount. Turnover frequencies (TOF) were determined by dividing the molar rate of CO_2 consumption by the molar amount of surface Cu.

3. Results

3.1 Catalyst Characterization

3.1.1 Morphology

The TEM images of CuSBA and rod-like SCuCe are shown in Figure 1(a) and (b). Cu nanoparticles are clearly present in the mesopores of SBA-15, as circled in Figure 1(a). Due to the

space-confined synthesis method, SCuCe and SCe were synthesized as rod-like structures, similar to the mesopores of SBA-15. In fact, the rod diameter of SCuCe was about 6-9 nm, equivalent to the mesopore diameter of the template SBA-15, suggesting that the salts were drawn into the mesopores of SBA-15 and that the template effectively confined the growth of the mixed metal oxides, thereby avoiding particle sintering caused by high calcination temperatures. Due to difficulty identifying Cu nanoparticles in Figure 1(b), elemental mapping of the sample was performed in conjunction with HAADF-STEM (High Angle Annular Dark Field). Figures 1(c) to (f), to show the elemental dispersion of SCuCe. The presence and distribution of elements Ce and Cu, as shown in Figure 1(e) and (f), respectively, suggest that Cu was highly dispersed on these materials, as expected.

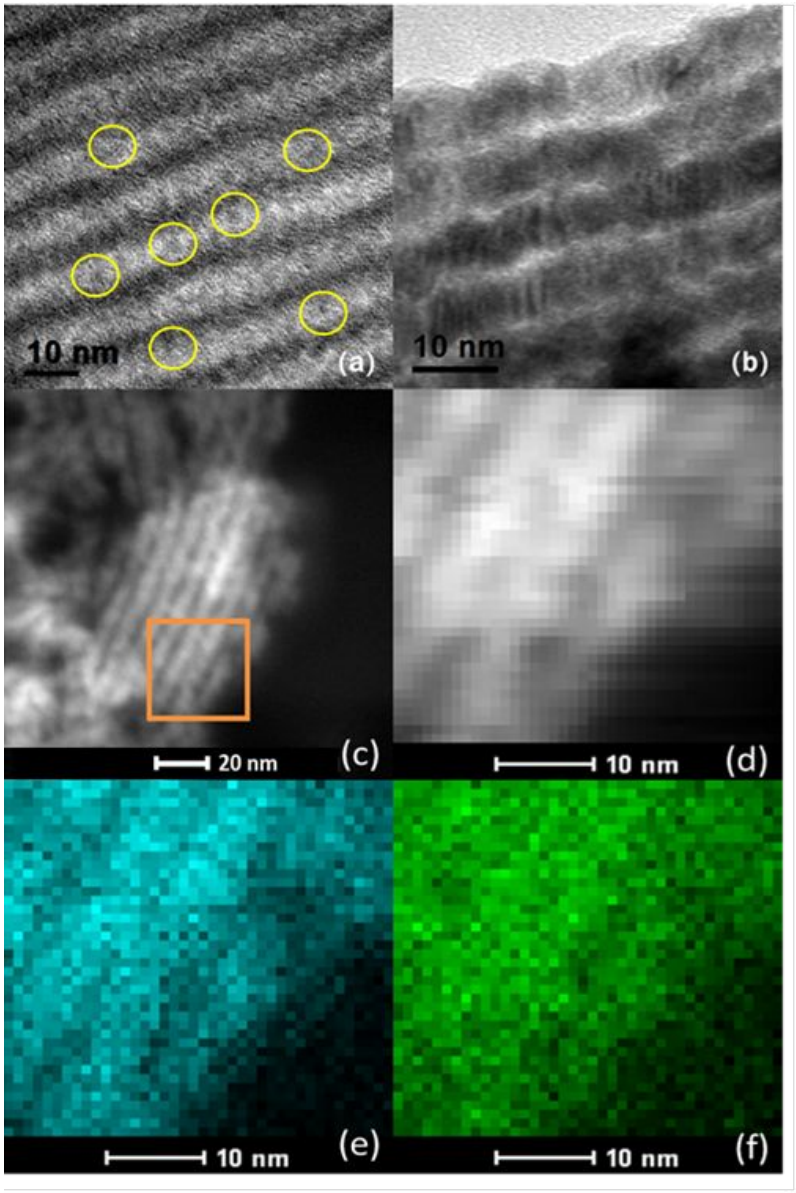

Figure 1. TEM images of (a) CuSBA, (b) SCuCe; (c) HAADF-STEM image of SCuCe, (d) a selected area of SCuCe for elemental mapping, (e) the Ce signal and (f) the Cu signal.

3.1.2 XRD

The in-house XRD patterns of the rod-like SCe and SCuCe, together with samples of CuSBA and bare SBA-15 are shown in Figure 2. The rod-like SCe and SCuCe have small Ce crystallite sizes, as seen from TEM (~8 nm). The characteristic reflections of CeO_2 in SCe and SCuCe are broad,

confirming the small particle size and demonstrating that using the space-confined synthesis method with a mesoporous template can produce CeO_2 nanoparticles while avoiding particle sintering at high calcination temperatures (>700 °C). There were no reflections attributable to CuO or Cu after calcination or after reduction (sample SCuCe-re), suggesting that the Cu domains were either amorphous or too small to be detected by the in-house XRD, in agreement with TEM results. Similar observations were made for the SBA-15 sample, Figure 2(b).

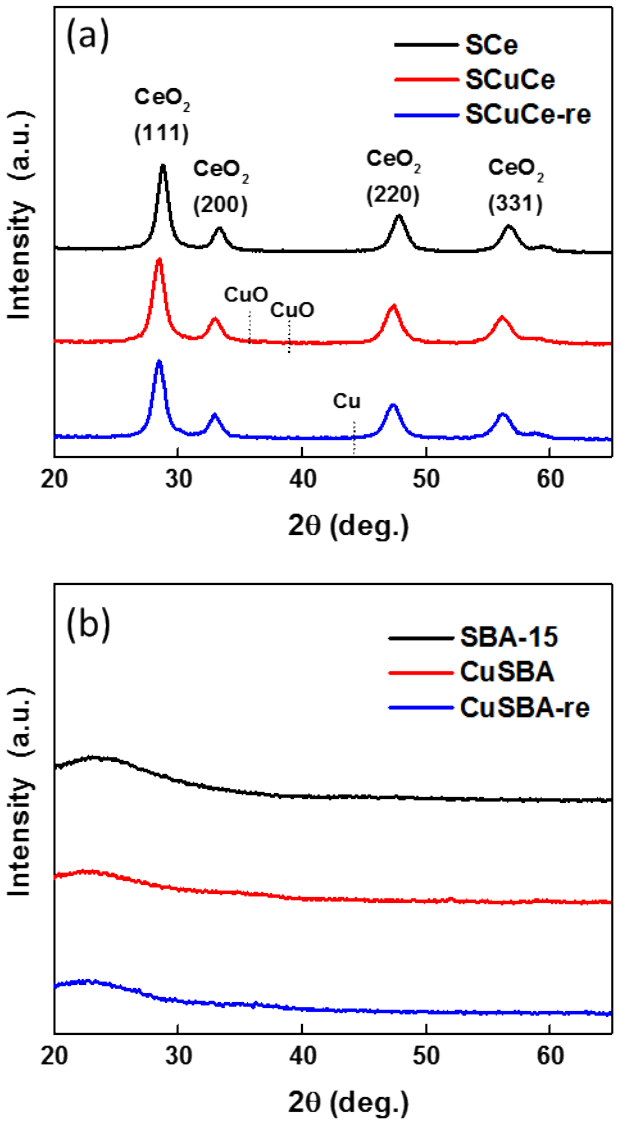

Figure 2. XRD patterns of (a) SCe and SCuCe and (b) CuSBA before and after the hydrogen reduction at 300 °C. Reduced samples are denoted as "-re".

In-situ XRD was performed using a synchrotron radiation light source to study the transformation of the rod-like oxide pre-catalyst $CuCeO_X$ (sample SCuCe) to CeO_2 and Cu, under reduction conditions from 25 to 300 °C, as shown in Figure 3. Between 25 and 120 °C, there was no significant difference in the positions of the CeO_2 reflections. Between 150 and 210 °C, all of the CeO_2 reflections shifted to lower angles, and a reflection attributable to Cu(111) appeared at 43.32°. After reduction at 300 °C and cooling to 25 °C, the (111), (200), and (220) reflections were shifted from 28.52° to 28.40°, 33.07° to 32.92° and 47.44° to 47.25°, respectively. The shifts to lower angles can be attributed to the partial reduction of Ce^{4+} to Ce^{3+}, which has a larger ionic radius than Ce^{4+}, and formation of an oxygen vacancy.[36] The oxygen vacancy formation process is facilitated by a simultaneous condensation of two electrons into the localized f-level traps on two cerium atoms. Thus, when an oxygen vacancy is created, these electrons localize on cerium atoms in the immediate surroundings of the vacancy.[37] The formation of reduced oxides can be understood as a formation, migration and ordering of virtual Ce^{3+}-vacancy complexes. We hypothesize that formation of these vacancies is facilitated by hydrogen spillover[38-40] from Cu to CeO_2, whereby an increased amount of reactive hydrogen molecules can be adsorbed and dissociated by the metal catalyst. The diffusion of hydrogen atoms from the metal catalyst onto the oxide support allows facile reduction of the oxide in the presence of the metal. Thus, from the *in-situ* XRD results, formation of Cu nanoparticles and

reduction of CeO_2 to form oxygen vacancies occur at the same time.

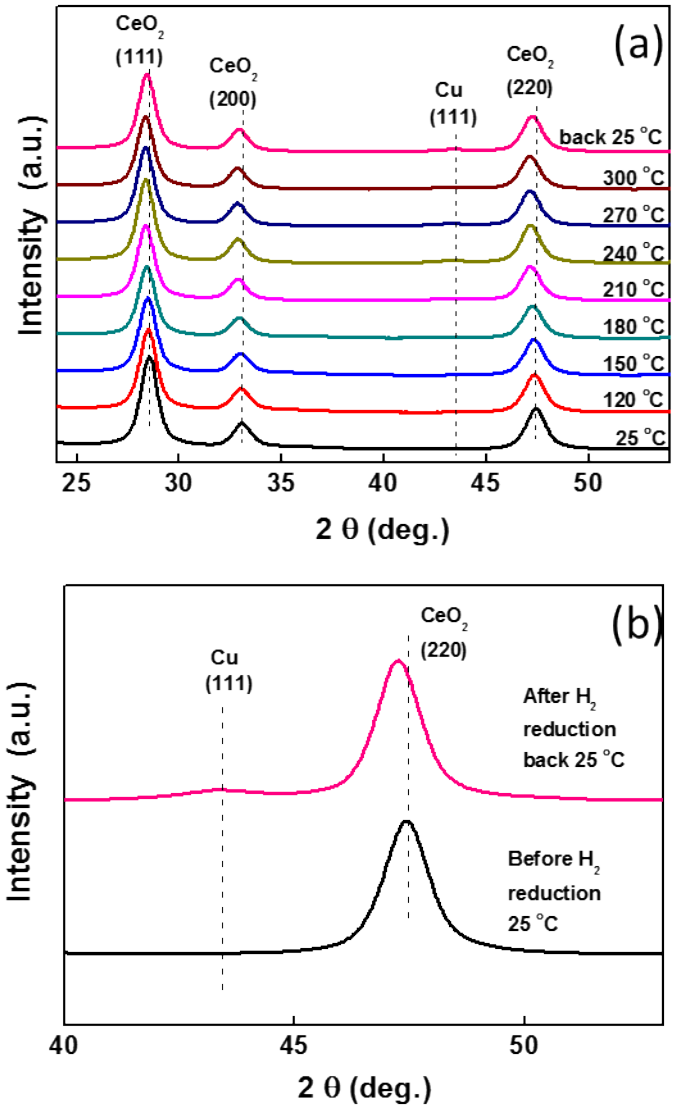

Figure 3. (a) *In-situ* XRD during H_2 reduction of SCuCe. (b) The shift in the CeO_2(220) reflections to lower angle and the emergence of the Cu(111) peak can be seen, suggesting simultaneous partial reduction of Ce^{4+} to Ce^{3+} and formation of Cu nanoparticles.

3.1.3 Cu K-edge XAS

The calibrated Cu K-edge X-ray absorption spectra for Cu foil, SCuCe-re and CuSBA-re are shown in Figure 4. The edge energy of the reference Cu foil is 8979 eV, which corresponds to an absorption threshold resonance, assigned to the transition from the 1s to 4p orbital.[41] After reduction by H_2 at 300 °C, the XANES features include a similar pre-edge as the Cu foil, at 8981 eV. In the EXAFS range, both of samples show less oscillations than the foil, reflecting the effect of metal domain size, as shown in Figure 4(a).

The Fourier-transformed (FT) data and corresponding fitting of the reduced samples SCuCe-re and CuSBA-re, as well as Cu foil, are shown in Figure 4(b) and the fitting parameters of Cu calculated from the Cu K-edge EXAFS are summarized in Table 1. From the Fourier-transformed EXAFS data, there is no evident Cu-O peak for SCuCe-re and CuSBA-re, and their Cu-Cu bond distance (2.52 Å) is similar with that of Cu foil (2.54 Å), suggesting that the reduction temperature of 300 °C was sufficient to fully reduce Cu. Additionally, the Cu-Cu coordination number in CuSBA-re and SCuCe-re were similar, at 8.5 and 8.7, respectively. In contrast, the Cu-Cu coordination number for Cu foil was 12.0, suggesting that the Cu nanoparticles produced on CuSBA-re and SCuCe-re are quite small (approximately 2 nm, as depicted in Figure S1).[38, 42] The dimensions and dispersion of Cu on support materials were further supported by TEM and N_2O chemisorption (see below), so that the size, amount and distribution of Cu nanoparticles in both samples were confirmed to be similar. Based on this premise, the influence of the metal-support synergy on the catalysis can be discussed exclusively.

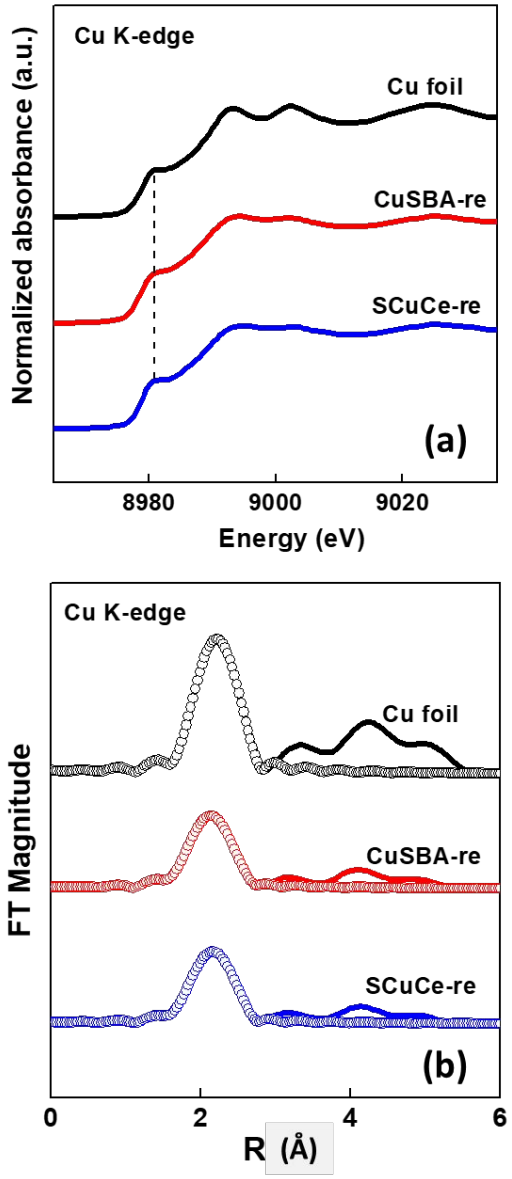

Figure 4. X-ray absorption spectra at the Cu K-edge of SCuCe and CuSBA after reduction, and Cu foil. XANES of (a), and FT-EXAFS with fitting (open line) of (b).

Table 1. Cu fitting parameters of the EXAFS data for CuSBA-re, SCuCe-re and Cu foil.

Sample	Shell	N	R (Å)	σ^2 ($\times 10^{-3}$) (Å^2)	r-factor
CuSBA-re	Cu-Cu	8.5 (±1.2)	2.52 (±0.01)	10.5 (±1.5)	0.003
SCuCe-re	Cu-Cu	8.7 (±1.3)	2.52 (±0.01)	10.7 (±1.4)	0.002
Cu foil	Cu-Cu	12.0 (±0.9)	2.54 (±0.01)	8.4 (±0.7)	0.0005

N: Coordination number, R: bond distance in Å and σ^2: Debye-Waller factor in Å^2

3.1.4 Ce L3-edge XANES

The calibrated Ce L3-edge XANES for SCe and SCuCe are shown in Figure 5(a) and (b), respectively. *In-situ* measurements were performed during sample reduction by hydrogen at 300 °C. The absorption energies at 5728 eV and 5733 eV correspond to a 2p to 5d transition, designated as the white line for $Ce^{3+}$and Ce^{4+}, respectively.[43] In Figure 5(a), no change was observed in the Ce L3-edge of SCe after hydrogen reduction, whereas partial reduction of Ce^{4+} to Ce^{3+} was observed for SCuCe, as seen in Figure 5(b). Quantification of the Ce^{3+} amount was performed by normalizing the Ce L3-edge XANES, subtracting the arctangent background, and fitting Gaussians functions.[44] Additional details for the fitting procedure can be found in the Supporting Information (Figure S2 and Table S2). This analysis suggests that the presence of Cu facilitated the reduction of Ce^{4+} to Ce^{3+}, with the amount of Ce^{3+} increasing significantly after reduction for the SCuCe-re sample, from 6.5% to 12.4%. These results are consistent with *in-situ* XRD data, which also suggest formation of Ce^{3+} and oxygen vacancies during hydrogen reduction of SCuCe, facilitated by Cu nanoparticles.

This also suggests that during the rWGS reaction, the filled oxygen vacancies at the interface may be recycled via regeneration in H_2 rich environments (H_2/CO_2 = 3/1).

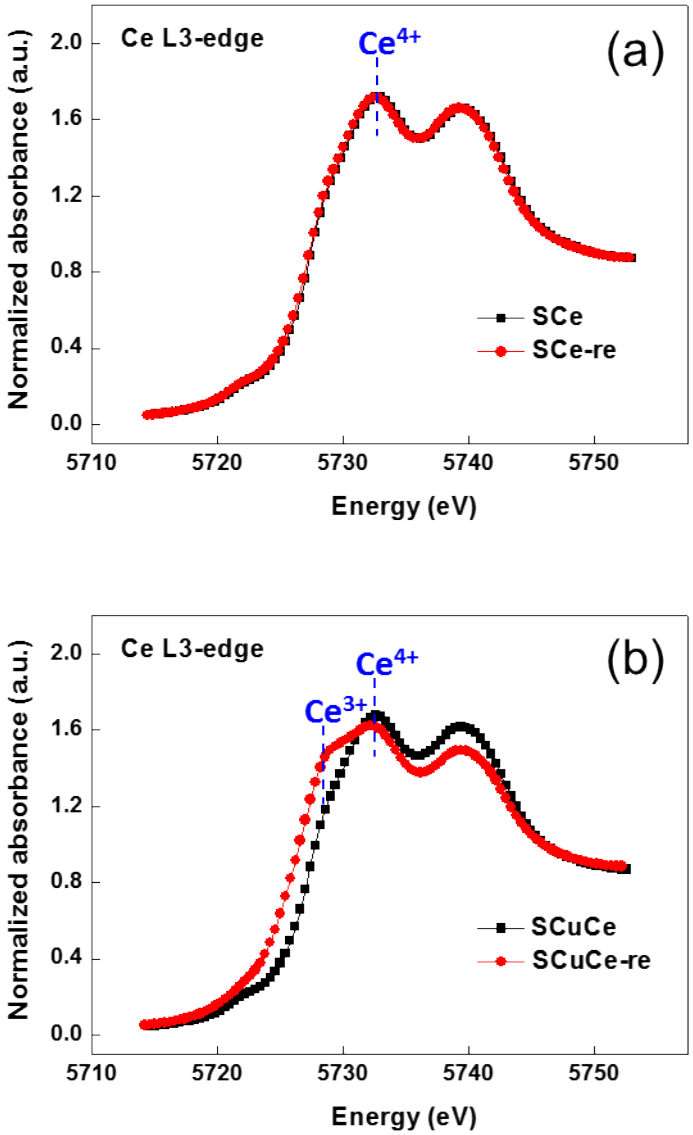

Figure 5. XANES at the Ce L3-edge of the samples before and after hydrogen reduction at 300 °C: (a) SCe and (b) SCuCe.

3.1.5 H_2 TPR and N_2O Chemisorption

H_2 temperature-programmed reduction (TPR) and N_2O chemisorption were performed to

determine the dispersion of Cu, calculated by comparing the amount of H_2 consumed in two separate experiments. The oxidized catalyst was subjected to TPR to calculate the total amount of Cu available. However, this experiment includes H_2 consumption from reduction of bulk CuO and partial reduction of CeO_2 (as shown by *in-situ* XRD and Ce L3-edge XANES experiments). Therefore, to calculate dispersion, the value for total Cu from ICP was used. After complete reduction, the sample was exposed to pulses of N_2O to oxidize the surface, and then H_2 TPR was conducted again. Since a monolayer of Cu_2O forms on the surface from exposure to N_2O,[45] the amount of surface Cu can be calculated, and the dispersion of copper can be derived accordingly. As shown in Table 2, the dispersion for both SCuCe and CuSBA was approximately 45-55%, suggesting particles approximately 2-3 nm in diameter, in agreement with TEM, XRD, and XAS. The TPR and detailed calculations (Figure S3 and Table S3) are shown in the supplementary information.

Table 2. Cu dispersion and turnover frequency estimates by hydrogen reduction at 300 °C using samples oxidized by N_2O chemisorption

Catalyst	Cu (wt%)	Dispersion (%)	TOF (h^{-1})	CO formation rate (mmol CO $\times h^{-1} \times g_{cat}^{-1}$)
SCuCe	9.0	53.8	8.7	6.6
CuSBA	8.9	45.2	2.2	1.4

3.2 Reaction of CO_2 to CO

3.2.1 Catalytic performance

The rWGS reaction was used to evaluate the catalyst performance, as shown in Figure 6. At 300 °C and 1 bar with a 3-to-1 H_2 to CO_2 molar ratio, the thermodynamically-limited equilibrium

conversion is estimated to be 22.8% (Figure S4). Based on the characterizations above confirming similar weight loading and dispersion/particle size of Cu (~9 wt% and 2-3 nm), the primary difference between the catalyst materials is the support, with the CeO_2 support being reducible and therefore containing oxygen vacancies, and the SiO_2 support being comparably inert. At a fixed WHSV and catalyst loading (0.2 g), SCuCe-re had ~18% CO_2 conversion and ~100% CO selectivity, which was higher than CuSBA-re's ~6% CO_2 conversion and ~98% CO selectivity (2% methanol).

The turnover frequency (TOF) was calculated by dividing the steady-state rate of CO_2 consumption by the amount of surface Cu (Table 2). The amount of SCuCe-re was reduced to 0.05 g to achieve similar conversion to CuSBA-re relatively far from equilibrium, at around 7% conversion. SCuCe-re was approximately 4 times more active than CuSBA-re, despite having similar Cu loading and dispersion. Therefore, it is likely that the reducibility of the CeO_2 support plays a role in assisting the catalytic reduction of CO_2 to CO, possibly by forming other active sites such as oxygen vacancies in the oxide support.

Samples were also evaluated at lower temperatures, as shown in Figure 6(c). Below 150 ^oC, both samples did not display quantifiable reactivity. SCuCe-re had ~3% and ~6% conversion at 200 and 250 ^oC, respectively, with ~100% CO selectivity. CuSBA-re had ~1% conversion at 250 ^oC with ~100% CO selectivity.

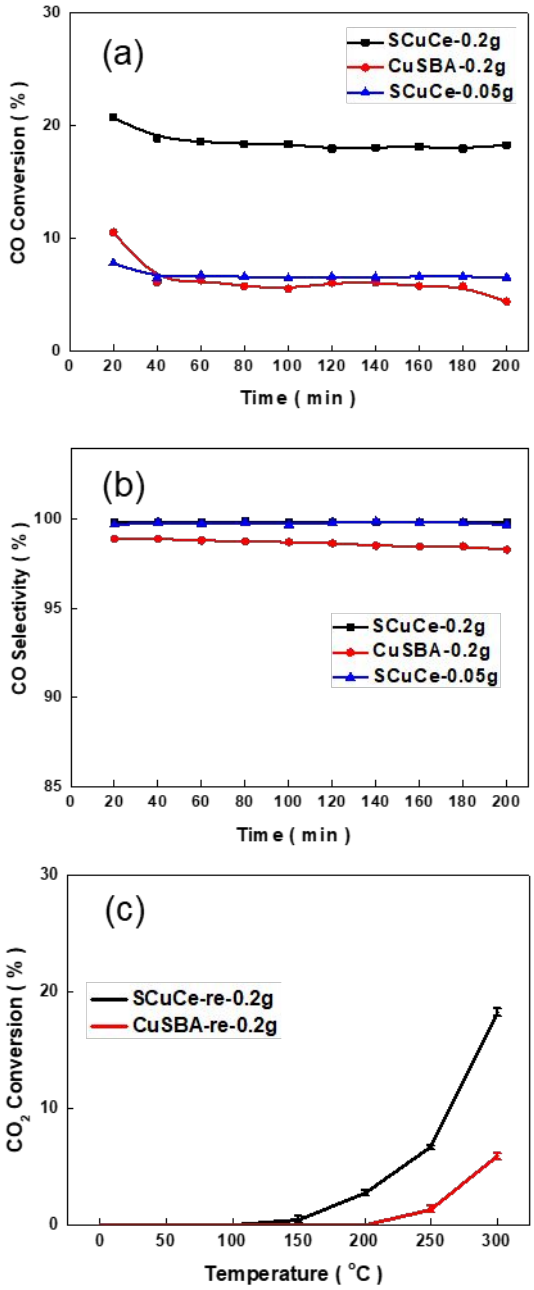

Figure 6. rWGS reaction of SCuCe-re and CuSBA-re. (a) CO_2 conversion; (b) CO selectivity. Reaction conditions: weight hourly space velocity (WHSV) of 1.08 or 4.32 h^{-1}, H_2/CO_2 molar ratio of 3, 300 °C and 1 bar. (c) CO_2 conversion as the reaction temperatures (50 to 300 °C).

3.2.2 *In-situ* FTIR

To probe the active sites involved in the conversion of CO_2 to CO, we used *in-situ* FTIR to

observe stable intermediates during CO_2 adsorption and desorption on the samples. Samples were first treated by H_2 reduction *in-situ* at 300 °C prior to reaction. Cooling to 35 °C and introduction of CO_2 to saturation leads to carbonate formation on ceria based catalysts, as noted in the literature,[30, 46] the experimental spectra were collected in the presence of the H_2 to probe carbonate hydrogenation at temperatures ranging from 35 to 300 °C. Several absorption bands appeared between 1700 to 1200 cm^{-1}, corresponding to carbonate or formate species; 2200 to 2100 cm^{-1} corresponding to carbonyl species; 3000 to 2700 cm^{-1} corresponding to formate species (C-H stretches); 3800 to 3500 cm^{-1} corresponding to hydroxyl species. The assignment of peaks to various species are summarized in Table 3. The evolution of various bands as a function of temperature was studied, and the spectra are shown in Figure 7.

Table 3. Adsorbed species of carbonate or formate on cerium oxide.

Group	Species assignment with ceria support	Frequencies observed (cm^{-1}) Literature (This work)
Carbonate[47-48]	Hydrogen Carbonate (HC)	1613(1618), 1391(1392) , 1218(1215)
	Bidentate Carbonate (B)	1562(1564), 1286(1295)
	Polydentate Carbonate (P)	1462(1470), 1353(1333)
Formate[47-48]	Bidentate Formate	2945, 2852(2842)
Carbonyl[48-51]	Ce^{4+}-CO	2175~ 2168
	Ce^{3+}-CO	2140~ 2120
	Cu^{2+}-CO	2160~ 2140
	Cu^{+}-CO	2117~ 2009(2112)
	Cu^{o}-CO	< 2100
Hydroxyl[47-48]	Ce^{4+}-OH (Type I)	3710(3729)
	Ce^{3+}-OH (Type II-B)	3651(3650)

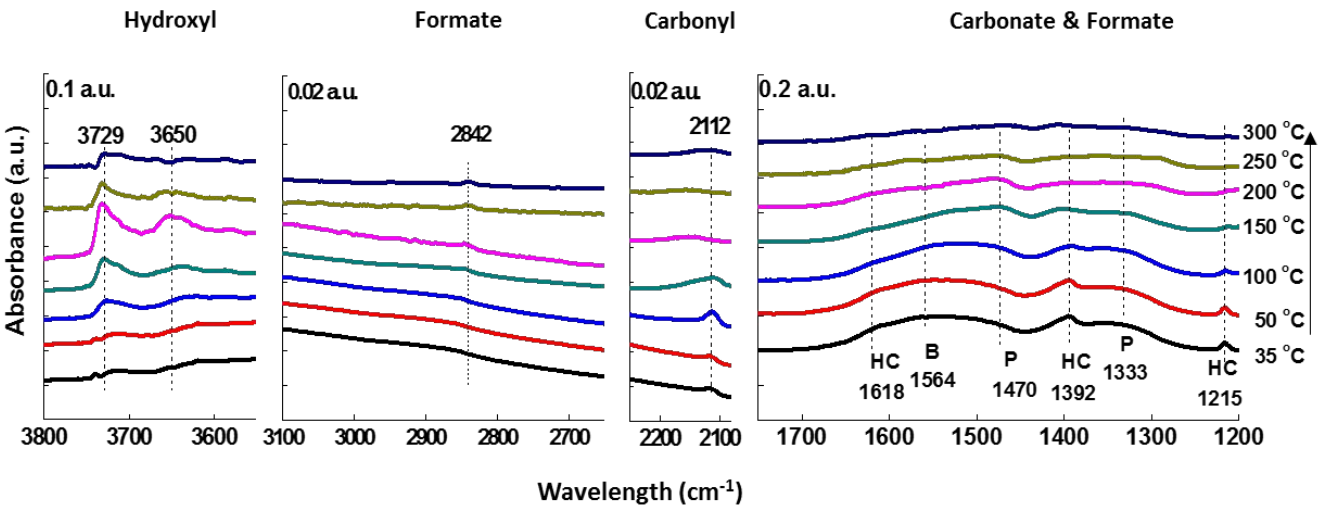

Figure 7. *In-situ* FTIR measurements of carbonate hydrogenation, whereby the SCuCe was initially reduced by H_2 (4% H_2 in He) at 300 °C and then background spectra were collected to eliminate the effect of temperature. After CO_2 introduction (1% CO_2 in He) leading to carbonate formation, the experimental spectra were collected in the presence of the same partial pressure of H_2 from 35 to 300 °C. He was used to purge the cell before every gas change.

CO_2 adsorption was observed on the reduced SCuCe catalyst with formation of hydrogen carbonate (1618, 1392, 1215 cm^{-1}), bidentate carbonate (1564 and 1300 cm^{-1}) and polydentate carbonate (1470, 1347 cm^{-1}) species at 35 °C. When the temperature of the system was increased from 35 to 300 °C, the intensity of all the carbonate bands decreased, suggesting the carbonate reacted or desorbed. A stretch at 2112 cm^{-1} was observed at 35 °C, which is normally assigned to Cu^{+}-CO[20, 48, 50] on the SCuCe-re catalyst. The formation of Cu^0 or Cu^{2+}-carbonyls was not observed, as expected, based on literature reports (Table 3). When the cell was heated to 100 °C, the intensity of the carbonyl stretch increased. This indicates that the carbonates are converted, with more obvious carbonyls detected at this temperature. As the temperature was first increased to 150 °C, the carbonyl stretch was observed to broaden, following by a decrease in intensity upon heating to 200 and then 300 °C. This

suggests that the carbonyls desorb or react at these higher temperatures. In comparison, the reference catalysts (SCe and CuSBA, containing CeO_2 and Cu alone, respectively) did not show any obvious carbonyl stretches throughout, as shown in Figure S6, suggesting that these species were either not formed, or desorbed immediately upon formation.

The investigation of the hydroxyl region provides additional information about the species formed during the rWGS reaction. The bands at 3729 and 3650 cm^{-1} are assigned to mono-coordinated hydroxyls on Ce^{4+} (Type I) and doubly bridging hydroxyls on Ce^{3+} (Type II-B), respectively.[47-48] At 150 °C, both of these bands were prominent, corroborating the XAS results (Figure 5) that Ce^{4+} is reduced to Ce^{3+} during reaction. As the temperature is increased from 250 to 300 °C, the intensity of these bands decreased, suggesting the hydroxyls desorbed at higher temperatures. These bands were not observed on the reference ceria without Cu (SCe, Figure S6), suggesting that the presence of Cu facilitated reduction of Ce. The C-H stretch of formate was assigned at 2842 cm^{-1}. At temperatures below 200 °C, there was no obvious formate stretch. However, a low intensity band appeared in the 200 to 300 °C temperature range.

3.2.3 Cu to Cu^+ and Ce^{3+} to Ce^{4+} via CO_2

CO_2 treatment of the SCuCe reduced catalyst was probed via *in-situ* XAS measurements to identify possible Cu structure changes, as shown Figure 8. After reduction, the sample exposed to CO_2 treatment at 120 °C is noted "-re 120 °C_CO_2". The observed spectral changes are compared with CuO and Cu_2O standards. In the Figure 8 (a), the pre-edge of the CO_2 treated sample is at 8982 eV, the same with the pre-edge energy of the Cu_2O standard. Fourier-transformed (FT) data and the corresponding fittings of the CO_2 treated sample, along with comparisons with CuO and Cu_2O standards are shown in Figure 8(b). The fitting parameters of Cu-O calculated from the Cu K-edge EXAFS are summarized in Table 4. The bond distance of the reduced catalyst after CO_2 treatment was 1.86 Å, which is similar to the Cu_2O standard (1.85 Å); the CuO standard had a bond distance of 1.94 Å. These results indicate that the Cu^0 species in SCuCe-re can be oxidized to Cu^+ species via CO_2

treatment at 120 °C. This result supports the *in-situ* FTIR measurements identifying observation of a Cu^{+}-CO stretch.

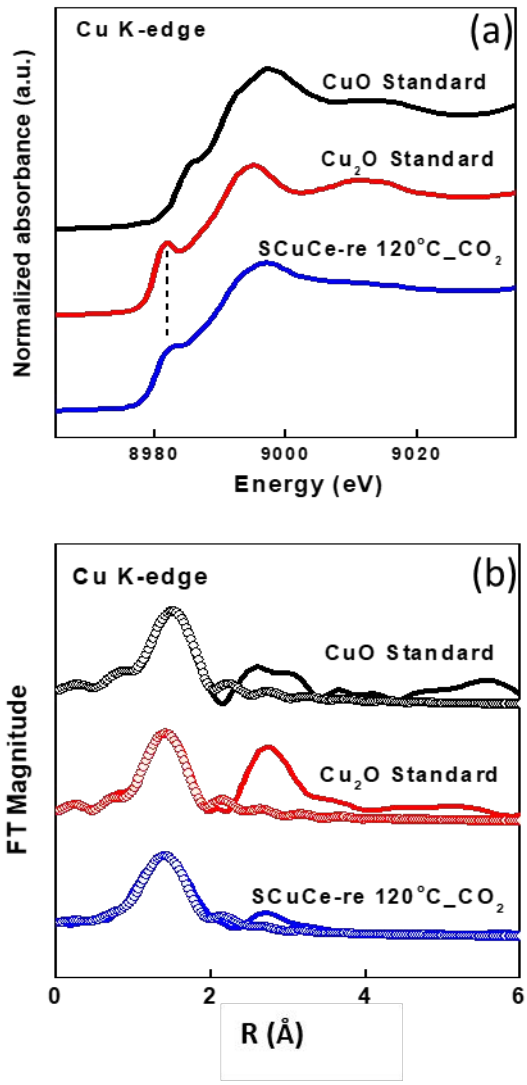

Figure 8. X-ray absorption spectra at the Cu K-edge of pre-reduced SCuCe after treatment with CO_2 at 120 °C (blue, SCuCe-re 120°C_CO_2). These *in-situ* data are compared with CuO (black) and Cu_2O (red) standards. XANES data are shown in (a), and FT-EXAFS data with a fitting (solid line) are shown in (b).

Table 4. Cu-O fitting parameters of the EXAFS data for CuO and Cu_2O standards, and CO_2 treated SCuCe-re.

Sample	Shell	N	R (Å)	σ^2 ($\times 10^{-3}$) (Å^2)	r-factor
CuO Standard	Cu-O	2.8 (±0.4)	1.94 (±0.02)	4.2 (±1.8)	0.006
Cu_2O Standard	Cu-O	1.6 (±0.1)	1.85 (±0.01)	2.2 (±1.2)	0.002
SCuCe-re 120 $^oC_CO_2$	Cu-O	1.4 (±0.2)	1.86 (±0.02)	7.5 (±3.2)	0.013

N: Coordination number, R: bond distance in Å and σ^2: Debye-Waller factor in Å^2

In parallel with the changes to the Cu oxidation state, the Ce^{3+} changes during the *in-situ* measurements are shown in Figure 9. The shoulder peak of 5728 eV is assigned to the Ce^{3+} species. After the H_2 reduction treatment, the intensity of the shoulder peak grew to be higher than that for the non-reduced sample; this indicates Ce^{3+} formation, as noted in the previous discussion. Next, the sample was continuously exposed to CO_2 at 120 ^{o}C, and the shoulder peak decreased in intensity compared to the reduced sample, but the intensity remained higher than that of the sample prior to reduction. This suggests that during the CO_2 treatment, the Ce^{3+} of the SCuCe-re participated in the reaction and was oxidized via CO_2 to Ce^{4+}. The steady state catalytic performance at 300 ^{o}C suggests that the oxygen vacancies of CeO_X can be regenerated by hydrogen spillover from Cu sites.

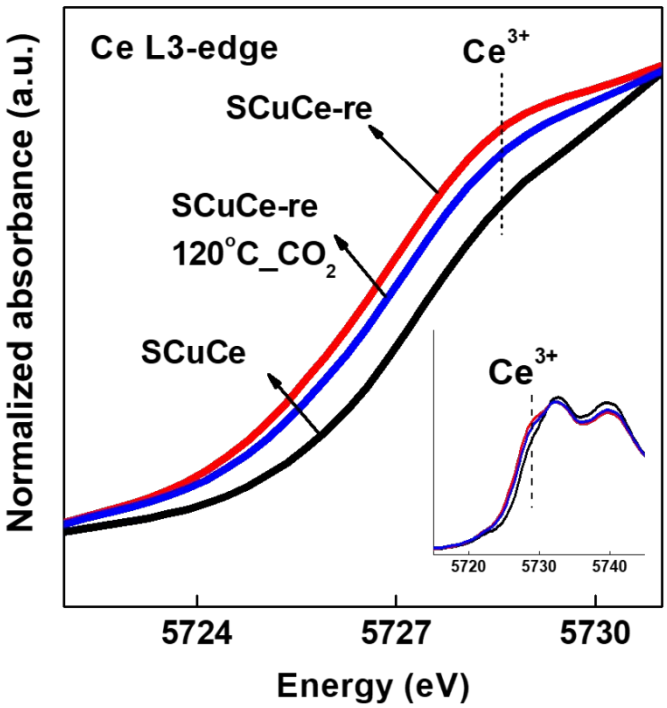

Figure 9. XANES at the Ce L3-edge of SCuCe, for the as-synthesized SCuCe, reduced SCuCe-re, and after CO_2 treatment at 120 °C SCuCe-re 120°C_CO_2.

4. Discussion

Based on the experimental data, the surface reactions and changes in the oxidation state of the catalyst can be understood as a function of reaction temperature. When the reaction temperatures were < 150 °C, no products of rWGS were detected by GC. However, changes in the organic species on the surface of the catalyst, and changes in the electronic state of the catalyst were observed. The *in-situ* FTIR measurements showed formation of Cu^{+}-CO intermediates at 100 to 150 °C, suggesting that at low temperatures, CO_2 is able to adsorb, dissociate and oxidize Cu^{0}. The existence of Cu^{+} was supported by *in-situ* XAS measurements. In parallel, Ce^{3+} can be oxidized to Ce^{4+}, as observed in the *in-situ* XAS, which suggests that the reaction may take place at the copper-ceria interface. When the

reaction temperature was > 150 °C, CO and H_2O were detected as products by GC during the rWGS reaction. In the *in-situ* FTIR spectra, the Cu^+-CO rapidly disappeared at elevated temperatures, the hydroxyl groups formed and desorbed, and a slight C-H stretch formed as the temperature as increased. We note that the *in-situ* FTIR provides only supporting, not definitive, evidence of the proposed reaction pathway; operando measurements are needed to make definitive assignments about kinetically relevant intermediates in the reaction pathways.[46] Nonetheless, the *in-situ* FTIR and GC results provide experimental evidence to support a density functional theory (DFT)-derived sequence of intermediates formed during CO_2 hydrogenation over ceria based catalysts.[30]

Our work suggests a sequence of formation in key species in the hydrogenation of CO_2 to methanol over Cu/CeO_2 catalysts. We note there was no obvious formate stretch (C-H) < 200 °C in the IR spectra, with these species then appearing in the 200 to 300 °C range, and there were not any formate products detected by GC analysis during these reaction temperatures. This may suggest that carbonyl formation can occur more easily and may occur prior to formate formation. Related to this, recent DFT studies[30, 52-53] describing the possible mechanisms of CO_2 hydrogenation to methanol over CeO_2 or metal-CeO_x catalysts showed that carbonate/carboxylate conversion to carbonyls occurred first, with the formyl to methoxy steps occurring subsequently, with the interface of metal and CeO_x being important. Our experimental data are consistent with these computational investigations.

In comparison, as reported by Jin et al.[51], on Pt-CeO_x with H_2 pre-treatment, CO_2 hydrogenation took place at the interface of Pt and CeO_x; the performance was, furthermore, better than that for CeO_2 or Pt alone. Meunier et al.[46] reported the reaction pathways for the rWGS over a Pt-CeO_x catalyst by steady-state isotopic transient kinetic analysis (SSITKA), which is an *operando* technique. They observed that the exchange time of the carbonates matched the rate of CO formation, suggesting the main reaction pathway was formation of CO from carbonates at ceria oxygen vacancies at the Pt-CeO_x interface. However, this was accompanied by formation of strongly-bound Pt-CO intermediates which persisted at the reaction temperature of 225 °C; suggesting the Pt-CO is not main intermediate in the pathway at these temperatures.

In our work, we observed oxidation of Cu to Cu^+ and formation of Cu^+-CO below 150 °C, with desorption of these intermediates above 150 °C. This suggests that the Cu-CeO_x catalyst has not only the interface sites (Cu-CeO_x) with oxygen vacancies, similar to Pt-CeO_x, but also a potential Cu^+-CO intermediate reaction pathway that may allow the Cu sites to be regenerated under mild conditions. We suggest the high reactivity over the SCuCe catalyst can be attributed to abundant interfaces between Cu nanoparticles on small CeO_x domain supports created by this particular catalyst synthesis method. The close proximity of Cu and the CeO_x support allows for facile reduction of the catalyst via hydrogen spillover, forming reduced species, Cu^0 and Ce^{3+} at the interface. When this reduced catalyst is exposed to CO_2, the CO_2 dissociates and oxidizes Cu^0 to Cu^+ and Ce^{3+} to Ce^{4+}, forming Cu^+-CO intermediates, among others. This intermediate rapidly desorbs at the reaction temperature of 300 °C, and the reduced sites can be regenerated rapidly by H_2 (Cu^+ to Cu^0) and hydrogen spillover (Cu^{4+} to Ce^{3+}), allowing for stable catalytic performance at mild conditions.

5. Conclusion

The reverse water-gas shift reaction over a Cu-CeO_x catalyst (SCuCe) created by a templating method was investigated and shown to approach the thermodynamically-limited equilibrium value with 100% CO selectivity at low reaction temperature (300 °C) and pressure (1 bar). Moreover, the catalyst was ~4 times more active than an equivalent Cu/SiO_2 catalyst at similar weight loading (~9 wt%, by ICP), metal particle size (~2 nm, by EXAFS), and Cu dispersion (~50%, by H_2/N_2O TPR). The improved catalytic performance is attributed to abundant interfaces formed between well-dispersed Cu nanoparticles and Ce^{3+} species, allowing for hydrogen spillover. CO_2 adsorption on reduced Cu/CeO_x and an observed change in Cu speciation (Cu^0 to Cu^+) associated with surface

intermediate formation (Cu^{+}-CO) at < 150 °C were identified by *in-situ* XAS and *in-situ* FTIR, respectively. In parallel, there was a lack of observed catalytic activity below this temperature. The parallel oxidation of Ce^{3+} to Ce^{4+} was also observed by the *in-situ* XAS. The rapid desorption of carbonyl and hydroxyl intermediates to form gas-phase CO and H_2O at temperatures > 200 °C was identified by *in-situ* FTIR and GC. The results are consistent with a reaction pathway similar to that proposed on Pt/CeOx catalysts in the literature, and supply experimental evidence for the existence of a Cu^{+}-CO intermediate under some conditions. In contrast to the Pt case, the Cu/CeOx catalysts are easily regenerated during reaction due to rapid desorption of CO after formation and facile reduction of both Cu and CeOx at the interface via hydrogen spillover. This approach can, in a principle, be combined with other processes, such as the Fischer–Tropsch reaction, to directly convert CO_2 to liquid fuels and other chemicals under the mild conditions.

Supporting Information

Supporting Information is available free of charge on the ACS Publications website at http://pubs.acs.org. Cu particle size evaluation by XAS, quantification of Ce^{3+}, N_2O chemisorption, *in-situ* FTIR of the SCe and CuSBA catalysts and catalytic activity of the supports are included.

Acknowledgements

S.-C. Y. thanks the Ministry of Science and Technology, Taiwan, for supporting the Postdoctoral Research Abroad Program (no. 105-2917-I-564-057). The Georgia Institute of Technology (GT),

National Taiwan University of Science and Technology (NTUST), as well as the facility support from the National Synchrotron Radiation Research Center (NSRRC) of BL01C, BL07C and BL17C are acknowledged. S.-C. Y. also thanks Prof. Shawn D. Lin for fruitful IR discussions (NTUST). Partial support was provided to S.J.P and C.W.J. by the Center for Understanding and Control of Acid Gas-Induced Evolution of Materials for Energy (UNCAGE-ME), an Energy Frontier Research Center, funded by U.S. Department of Energy (US DoE), Office of Science, Basic Energy Sciences (BES) under Award DE-SC0012577.

References

(1) Glikson, A., Cenozoic mean greenhouse gases and temperature changes with reference to the Anthropocene. *Glob. Change Biol.* **2016,** *22*, 3843-3858.

(2) Blunden, J.; Arndt, D. S., State of the Climate in 2013. *Bull. Am. Meteorol. Soc.* **2014,** *95*, S1-S279.

(3) Li, J.-R.; Ma, Y.; McCarthy, M. C.; Sculley, J.; Yu, J.; Jeong, H.-K.; Balbuena, P. B.; Zhou, H.-C., Carbon dioxide capture-related gas adsorption and separation in metal-organic frameworks. *Coord. Chem. Rev.* **2011,** *255*, 1791-1823.

(4) Choi, S.; Drese, J. H.; Jones, C. W., Adsorbent Materials for Carbon Dioxide Capture from Large Anthropogenic Point Sources. *ChemSusChem* **2009,** *2*, 796-854.

(5) Blamey, J.; Anthony, E. J.; Wang, J.; Fennell, P. S., The calcium looping cycle for large-scale CO_2 capture. *Prog. Energy Combust. Sci.* **2010,** *36*, 260-279.

(6) Sanz-Pérez, E. S.; Murdock, C. R.; Didas, S. A.; Jones, C. W., Direct Capture of CO_2 from Ambient Air. *Chem. Rev.* **2016,** *116*, 11840-11876.

(7) Celia, M. A.; Nordbotten, J. M.; Court, B.; Dobossy, M.; Bachu, S., Field-scale application of a semi-analytical model for estimation of CO_2 and brine leakage along old wells. *Int. J. Greenh Gas Con.* **2011,** *5*, 257-269.

(8) Aresta, M.; Dibenedetto, A.; Angelini, A., Catalysis for the Valorization of Exhaust Carbon: from CO_2 to Chemicals, Materials, and Fuels. Technological Use of CO_2. *Chem. Rev.* **2014,** *114*, 1709-1742.

(9) Wang, S.; Wang, X., Imidazolium Ionic Liquids, Imidazolylidene Heterocyclic Carbenes, and

Zeolitic Imidazolate Frameworks for CO_2 Capture and Photochemical Reduction. *Angew. Chem. Int. Ed.* **2016,** *55*, 2308-2320.

(10) Agarwal, A. S.; Zhai, Y.; Hill, D.; Sridhar, N., The Electrochemical Reduction of Carbon Dioxide to Formate/Formic Acid: Engineering and Economic Feasibility. *ChemSusChem* **2011,** *4*, 1301-1310.

(11) Porosoff, M. D.; Yan, B.; Chen, J. G., Catalytic reduction of CO_2 by H_2 for synthesis of CO, methanol and hydrocarbons: challenges and opportunities. *Energy Environ. Sci.* **2016,** *9*, 62-73.

(12) Hori, Y., Electrochemical CO_2 Reduction on Metal Electrodes. In *Modern Aspects of Electrochemistry*, Vayenas, C. G.; White, R. E.; Gamboa-Aldeco, M. E., Eds. Springer New York: New York, NY, 2008; pp 89-189.

(13) Centi, G.; Perathoner, S., Opportunities and prospects in the chemical recycling of carbon dioxide to fuels. *Catal. Today* **2009,** *148*, 191-205.

(14) Chen, C.-S.; Cheng, W.-H.; Lin, S.-S., Study of reverse water gas shift reaction by TPD, TPR and CO_2 hydrogenation over potassium-promoted Cu/SiO_2 catalyst. *Appl. Catal., A.* **2003,** *238*, 55-67.

(15) Arena, F.; Mezzatesta, G.; Zafarana, G.; Trunfio, G.; Frusteri, F.; Spadaro, L., Effects of oxide carriers on surface functionality and process performance of the Cu–ZnO system in the synthesis of methanol via CO_2 hydrogenation. *J. Catal.* **2013,** *300*, 141-151.

(16) Kim, S. S.; Park, K. H.; Hong, S. C., A study of the selectivity of the reverse water–gas-shift reaction over Pt/TiO_2 catalysts. *Fuel Process. Technol.* **2013,** *108*, 47-54.

(17) Gallego, G. S.; Mondragón, F.; Barrault, J.; Tatibouët, J.-M.; Batiot-Dupeyrat, C., CO_2 reforming of CH_4 over La–Ni based perovskite precursors. *Appl. Catal., A* **2006,** *311*, 164-171.

(18) Laachir, A.; Perrichon, V.; Badri, A.; Lamotte, J.; Catherine, E.; Lavalley, J. C.; El Fallah, J.; Hilaire, L.; Le Normand, F.; Quemere, E.; Sauvion, G. N.; Touret, O., Reduction of CeO_2 by hydrogen. Magnetic susceptibility and Fourier-transform infrared, ultraviolet and X-ray photoelectron spectroscopy measurements. *J. Chem. Soc., Faraday Trans.* **1991,** *87*, 1601-1609.

(19) Martínez-Arias, A.; Gamarra, D.; Fernández-García, M.; Hornés, A.; Bera, P.; Koppány, Z.; Schay, Z., Redox-catalytic correlations in oxidised copper-ceria CO-PROX catalysts. *Catal. Today* **2009,** *143*, 211-217.

(20) Gamarra, D.; Belver, C.; Fernández-García, M.; Martínez-Arias, A., Selective CO Oxidation in Excess H_2 over Copper−Ceria Catalysts: Identification of Active Entities/Species. *J. Am. Chem. Soc.* **2007,** *129*, 12064-12065.

(21) Yang, F.; Graciani, J.; Evans, J.; Liu, P.; Hrbek, J.; Sanz, J. F.; Rodriguez, J. A., CO Oxidation on Inverse CeOx/Cu(111) Catalysts: High Catalytic Activity and Ceria-Promoted Dissociation of O_2. *J. Am. Chem. Soc.* **2011,** *133*, 3444-3451.

(22) Yang, Z.; He, B.; Lu, Z.; Hermansson, K., Physisorbed, Chemisorbed, and Oxidized CO on Highly Active Cu−CeO_2(111). *J. Phys. Chem. C* **2010,** *114*, 4486-4494.

(23) Wang, X.; Rodriguez, J. A.; Hanson, J. C.; Gamarra, D.; Martínez-Arias, A.; Fernández-García, M., In Situ Studies of the Active Sites for the Water Gas Shift Reaction over Cu−CeO_2 Catalysts: Complex Interaction between Metallic Copper and Oxygen Vacancies of Ceria. *J. Phys. Chem. B* **2006,**

110, 428-434.

(24) Rodriguez, J. A.; Graciani, J.; Evans, J.; Park, J. B.; Yang, F.; Stacchiola, D.; Senanayake, S. D.; Ma, S.; Pérez, M.; Liu, P.; Sanz, J. F.; Hrbek, J., Water-Gas Shift Reaction on a Highly Active Inverse CeOx/Cu(111) Catalyst: Unique Role of Ceria Nanoparticles. *Angew. Chem. Int. Ed.* **2009,** *48*, 8047-8050.

(25) Mudiyanselage, K.; Senanayake, S. D.; Feria, L.; Kundu, S.; Baber, A. E.; Graciani, J.; Vidal, A. B.; Agnoli, S.; Evans, J.; Chang, R.; Axnanda, S.; Liu, Z.; Sanz, J. F.; Liu, P.; Rodriguez, J. A.; Stacchiola, D. J., Importance of the Metal–Oxide Interface in Catalysis: In Situ Studies of the Water–Gas Shift Reaction by Ambient-Pressure X-ray Photoelectron Spectroscopy. *Angew. Chem. Int. Ed.* **2013,** *52*, 5101-5105.

(26) Liu, Y.; Hayakawa, T.; Suzuki, K.; Hamakawa, S.; Tsunoda, T.; Ishii, T.; Kumagai, M., Highly active copper/ceria catalysts for steam reforming of methanol. *Appl. Catal., A* **2002,** *223*, 137-145.

(27) Yang, S.-C.; Su, W.-N.; Lin, S. D.; Rick, J.; Hwang, B.-J., Preparation of highly dispersed catalytic Cu from rod-like CuO-CeO_2 mixed metal oxides: suitable for applications in high performance methanol steam reforming. *Catal. Sci. Technol* **2012,** *2*, 807-812.

(28) Gu, X.-K.; Li, W.-X., First-Principles Study on the Origin of the Different Selectivities for Methanol Steam Reforming on Cu(111) and Pd(111). *J. Phys. Chem. C* **2010,** *114*, 21539-21547.

(29) Rodriguez, J. A.; Liu, P.; Stacchiola, D. J.; Senanayake, S. D.; White, M. G.; Chen, J. G., Hydrogenation of CO_2 to Methanol: Importance of Metal–Oxide and Metal–Carbide Interfaces in the Activation of CO_2. *ACS Catal.* **2015,** *5*, 6696-6706.

(30) Graciani, J.; Mudiyanselage, K.; Xu, F.; Baber, A. E.; Evans, J.; Senanayake, S. D.; Stacchiola, D. J.; Liu, P.; Hrbek, J.; Sanz, J. F.; Rodriguez, J. A., Highly active copper-ceria and copper-ceria-titania catalysts for methanol synthesis from CO_2. *Science* **2014,** *345*, 546-550.

(31) Senanayake, S. D.; Ramírez, P. J.; Waluyo, I.; Kundu, S.; Mudiyanselage, K.; Liu, Z.; Liu, Z.; Axnanda, S.; Stacchiola, D. J.; Evans, J.; Rodriguez, J. A., Hydrogenation of CO_2 to Methanol on CeOx/Cu(111) and ZnO/Cu(111) Catalysts: Role of the Metal–Oxide Interface and Importance of Ce3+ Sites. *J. Phys. Chem. C* **2016,** *120*, 1778-1784.

(32) Ouyang, B.; Tan, W.; Liu, B., Morphology effect of nanostructure ceria on the Cu/CeO_2 catalysts for synthesis of methanol from CO_2 hydrogenation. *Catal. Commun.* **2017,** *95*, 36-39.

(33) Yang, S.-C.; Su, W.-N.; Rick, J.; Lin, S. D.; Liu, J.-Y.; Pan, C.-J.; Lee, J.-F.; Hwang, B.-J., Oxygen Vacancy Engineering of Cerium Oxides for Carbon Dioxide Capture and Reduction. *ChemSusChem* **2013,** *6*, 1326-1329.

(34) Liu, C.-H.; Lai, N.-C.; Lee, J.-F.; Chen, C.-S.; Yang, C.-M., SBA-15-supported highly dispersed copper catalysts: Vacuum–thermal preparation and catalytic studies in propylene partial oxidation to acrolein. *J. Catal.* **2014,** *316*, 231-239.

(35) Zhao, D. Y.; Feng, J. L.; Huo, Q. S.; Melosh, N.; Fredrickson, G. H.; Chmelka, B. F.; Stucky, G. D., Triblock Copolymer Syntheses of Mesoporous Silica with Periodic 50 to 300 Angstrom Pores. *Science* **1998,** *279*, 548-552.

(36) Braglia, L.; Bugaev, A. L.; Lomachenko, K. A.; Soldatov, A. V.; Lamberti, C.; Guda, A. A.,

Investigation of oxygen vacancies in CeO_2 /Pt system with synchrotron light techniques. *J. Phys. Conf. Ser* **2016,** *712*, 012064.

(37) Skorodumova, N. V.; Simak, S. I.; Lundqvist, B. I.; Abrikosov, I. A.; Johansson, B., Quantum origin of the oxygen storage capability of ceria. *Phys. Rev. Lett.* **2002,** *89*, 1666011-1666014.

(38) Karim, W.; Spreafico, C.; Kleibert, A.; Gobrecht, J.; VandeVondele, J.; Ekinci, Y.; van Bokhoven, J. A., Catalyst support effects on hydrogen spillover. *Nature* **2017,** *541*, 68-71.

(39) Dutta, G.; Waghmare, U. V.; Baidya, T.; Hegde, M. S., Hydrogen Spillover on CeO_2/Pt: Enhanced Storage of Active Hydrogen. *Chem. Mater.* **2007,** *19*, 6430-6436.

(40) Trovarelli, A., Catalytic Properties of Ceria and CeO_2-Containing Materials. *Catal. Rev.* **1996,** *38*, 439-520.

(41) Eun, Y. C.; In-Sik, N.; Young, G. K.; Jong, S. C.; Jae, S. L.; Nomura, M., An X-ray absorption study of copper ion exchanged H-mordenite for selective catalytic reduction of NO by ammonia. *J. Mol. Catal.* **1991,** *69*, 247-258.

(42) Frenkel, A. I.; Hills, C. W.; Nuzzo, R. G., A View from the Inside: Complexity in the Atomic Scale Ordering of Supported Metal Nanoparticles. *J. Phys. Chem. B* **2001,** *105*, 12689-12703.

(43) Cafun, J.-D.; Kvashnina, K. O.; Casals, E.; Puntes, V. F.; Glatzel, P., Absence of Ce^{3+} Sites in Chemically Active Colloidal Ceria Nanoparticles. *ACS Nano* **2013,** *7*, 10726-10732.

(44) Nachimuthu, P.; Shih, W.-C.; Liu, R.-S.; Jang, L.-Y.; Chen, J.-M., The Study of Nanocrystalline Cerium Oxide by X-Ray Absorption Spectroscopy. *J. Solid State Chem.* **2000,** *149*, 408-413.

(45) Evans, J. W.; Wainwright, M. S.; Bridgewater, A. J.; Young, D. J., On the determination of copper surface area by reaction with nitrous oxide. *Appl. Catal.* **1983,** *7*, 75-83.

(46) Goguet, A.; Meunier, F. C.; Tibiletti, D.; Breen, J. P.; Burch, R., Spectrokinetic Investigation of Reverse Water-Gas-Shift Reaction Intermediates over a Pt/CeO_2 Catalyst. *J. Phys. Chem. B* **2004,** *108*, 20240-20246.

(47) Pozdnyakova, O.; Teschner, D.; Wootsch, A.; Kröhnert, J.; Steinhauer, B.; Sauer, H.; Toth, L.; Jentoft, F. C.; Knop-Gericke, A.; Paál, Z.; Schlögl, R., Preferential CO oxidation in hydrogen (PROX) on ceria-supported catalysts, part I: Oxidation state and surface species on Pt/CeO_2 under reaction conditions. *J. Catal.* **2006,** *237*, 1-16.

(48) Bera, P.; Priolkar, K. R.; Sarode, P. R.; Hegde, M. S.; Emura, S.; Kumashiro, R.; Lalla, N. P., Structural Investigation of Combustion Synthesized Cu/CeO_2 Catalysts by EXAFS and Other Physical Techniques: Formation of a Ce1-xCuxO2-δ Solid Solution. *Chem. Mater.* **2002,** *14*, 3591-3601.

(49) Daly, H.; Ni, J.; Thompsett, D.; Meunier, F. C., On the usefulness of carbon isotopic exchange for the operando analysis of metal–carbonyl bands by IR over ceria-containing catalysts. *J. Catal.* **2008,** *254*, 238-243.

(50) Martínez-Arias, A.; Fernández-García, M.; Gálvez, O.; Coronado, J. M.; Anderson, J. A.; Conesa, J. C.; Soria, J.; Munuera, G., Comparative Study on Redox Properties and Catalytic Behavior for CO Oxidation of CuO/CeO_2 and CuO/$ZrCeO_4$ Catalysts. *J. Catal.* **2000,** *195*, 207-216.

(51) Jin, T.; Zhou, Y.; Mains, G. J.; White, J. M., Infrared and x-ray photoelectron spectroscopy

study of carbon monoxide and carbon dioxide on platinum/ceria. *J. Phys. Chem.* **1987,** *91*, 5931-5937.

(52) Kumari, N.; Haider, M. A.; Agarwal, M.; Sinha, N.; Basu, S., Role of Reduced CeO_2(110) Surface for CO_2 Reduction to CO and Methanol. *J. Phys. Chem. C* **2016,** *120*, 16626-16635.

(53) Guo, C.; Wei, S.; Zhou, S.; Zhang, T.; Wang, Z.; Ng, S.-P.; Lu, X.; Wu, C.-M. L.; Guo, W., Initial Reduction of CO_2 on Pd-, Ru-, and Cu-Doped CeO_2(111) Surfaces: Effects of Surface Modification on Catalytic Activity and Selectivity. *ACS Appl. Mater. Inter.* **2017,** *9*, 26107-26117.

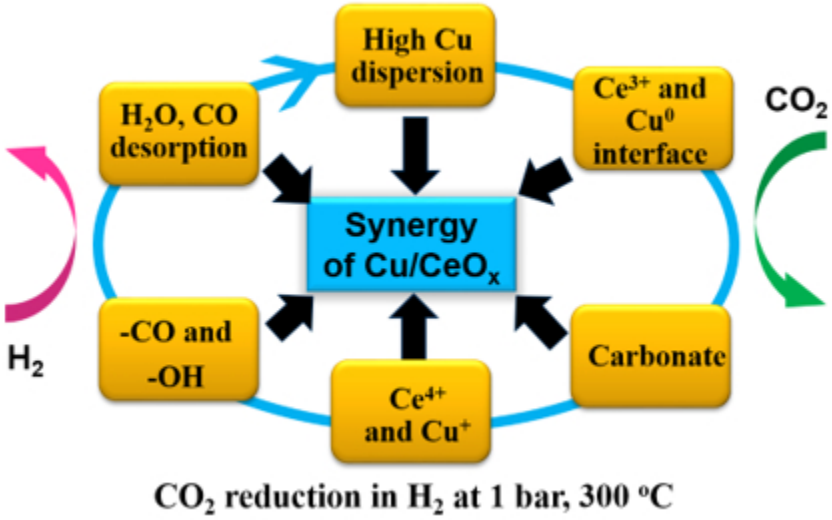

TOC graphic

78x47mm (150 x 150 DPI)